https://doi.org/10.5194/tc-2023-26
Preprint. Discussion started: 21 February 2023

The Cryosphere Discussions

Ice plate deformation and cracking revealed by an in-situ distributed acoustic sensing array

Jun Xie[1], Xiangfang Zeng[1], Chao Liang[2], Sidao Ni[1], Risheng Chu[1], Feng Bao[1], Rongbing Lin[1], Benxin Chi[1], Hao Lv[1]

[1] State Key Laboratory of Geodesy and Earth's Dynamics, Innovation Academy for Precision Measurement Science and Technology, Chinese Academy of Sciences, Wuhan, 430077, China
[2] Institute for Disaster Management and Reconstruction (IDMR), Sichuan University, Chengdu, 610100, China

Correspondence to: Xiangfang Zeng (zengxf@whigg.ac.cn)

Abstract. The study of seismic sources and wave propagation in ice plate is helpful to understand the structure, migration, fracture mechanics, mass balance and other processes. However, due to extreme environment, in-situ dense seismic observations are rare and the dynamic changes of the ice plate remain poorly understood. We conduct a seismic experiment with distributed acoustic sensing array on a frozen lake. We excite water vibrations by under-water airgun shots. With an artificial intelligence method, we detected seismic signals including high frequency icequakes and low frequency events. Icequakes cluster along the fractures and correlate with the local temperature variation. The flexural-gravity wave reveals the property of the ice plate. Our study demonstrates the utility of DAS array as an in-situ dense seismic network in illuminating the internal failure process and dynamic deformation of ice plate such as ice shelf, which contributes to understanding and prediction of disintegrations of ice shelves.

1 Introduction

Cryo-seismology can provide high temporal resolution results for the study of glacier dynamics, thus attracting the attention of scientists from seismology, cryosphere and climatology (Aster and Winberry, 2017; Podolskiy and Walter, 2016). Seismological records of the cryosphere can be used to study the dynamic process of the surface or interior of the glacier, so as to reveal the ice shelf damage, environmental changes and other fields. Large glacial earthquakes can be recorded by almost global networks (for example GSN), and they have been well studied to inferring the process of iceberg calving and capsizing (Ekström et al., 2003; Sergeant et al., 2019; Veitch and Nettles, 2017). However, local microseismicities (such as crevasse opening and development) can better reveal the dynamic change process of glaciers and be used to study the mechanism of glacier disintegration (Helmstetter et al., 2015; Lombardi et al., 2019; Romeyn et al., 2021; Walter et al., 2013). Due to low seismic energy and high attenuation, we need close stations (e.g., on the ice surface or in shallow boreholes) (Röösli et al., 2014; West et al., 2010). However, the complex environment and heavy logistics of glaciers make it difficult to install in situ seismometers. Some researchers even studied the potential of using one single seismometer to study icequakes (Köhler et al., 2019).

https://doi.org/10.5194/tc-2023-26
Preprint. Discussion started: 21 February 2023


The Cryosphere Discussions

In recent years, the distributed acoustic sensing (DAS) array with advantage of large aperture and dense observation has been tested on glacier environment to study the glacial structure and detect its seismicities (Booth et al., 2020; Brisbourne et al., 2021; Castongia et al., 2017; Fichtner et al., 2022; Hudson et al., 2021; Walter et al., 2020). Hudson et al. (2021) explored using DAS to monitor basal icequakes at Rutford Ice Stream. They compared the performance of DAS with geophone network for microseism detection and location. And found the DAS is superior for recording the microseism signal. Their methodology and implications are heuristic for the applying of DAS in glacial environment. Walter et al. (2020) deployed DAS in Alpine terrain and detected glacier stick-slip event related with glacier flow and nearby rock falls. Their work demonstrated the potential of DAS technology for seismic monitoring of glacier dynamics and natural hazards in the mountain region. These work demonstrated logistical feasibility of installing a large, high-quality DAS network in a glacial environment.

In this study, we deploy a DAS network on a frozen lake, the Xiliushui Reservoir in Gansu Province, China to investigate the utility of a DAS array in monitoring the cracking and dynamic flexure of ice plate (Fig. 1). Seismicity has been observed on frozen lake similar to icequakes in ice shelf (Dobretsov et al., 2013; Kavanaugh et al., 2018; Ruzhich et al., 2009). Nziengui-Bâ et al. (2022) measured the thickness and Young's modulus of the ice pack of a lake with DAS. Fichtner et al. (2022) deployed optical fiber on a frozen lake of a volcano. They detected the volcanic tremor. We excite water waves using an underwater AirGun Excitation (AGE), and record the vibration of water. Using an AI based method we detect and classify the abundant seismic events including both icequakes and Low Frequency Events (LFEs). We then analyze the characteristics and physical mechanism of the seismic signals through the waveform, occurrence rate and location. The stiffness of the ice plate is estimated with the dispersion of the flexural-gravity wave excited by LFEs. Finally, we discuss implication of our experiments for studying ice shelf dynamics in nature.

2 Experimental setting

The experimental site is at the Zhangye airgun active source platform, which is in Xiliushui Reservoir, the secondary reservoir of Zhangye Longshou Hydropower Station in Qilian Mountain, Zhangye City, Gansu Province, China (Fig. 1). The average elevation of the platform is ~1900 meters. The water depth of the lake is 45-65 meters, and the ice thickness in the reservoir is ~0.5 meters in North Hemisphere winter. The active airgun source is located in the centre of the lake at a depth of 15 meters blow the water (Wei et al., 2018). Bubbles excited by the airgun can produce water vibration (de Graaf et al., 2014), which is a good active source for simulating ocean waves.

A 1.2 km optical cable was deployed on the surface of the ice from January 6th to January 9th, 2020. The optical cable laid around the airgun floating platform in two circles. The inner circle is about 340 m long (channels 470-645), and the outer circle is nearly 800 m long (channels 51-457) (Fig. 1). We poured the optical cable with water, as the water froze, the optical cable was well coupled with the ice surface. In this experiment, the gauge length is 10 m, the spatial sampling

https://doi.org/10.5194/tc-2023-26
Preprint. Discussion started: 21 February 2023

interval is 2 m, and the temporal sampling rate is 1000 Hz. The experiment started at 21:00 p.m. on January 6th (Beijing time) and ended at 17:00 p.m. on January 9th. Some instrument failures occurred in the afternoon of January 8th, and there was no complete record from 11:00 p.m. to 13:00 p.m. A total of 65 hours of nearly 2 TB of data was recorded. In addition, there was a CMG-40T three-component short-period seismometer with a RefTek 130B data logger on the shore to record ground motion, with a sampling rate of 50 Hz.

3 Seismic events

During the experiment, 239 AGEs were carried out in total. Due to the instrumental issue, only 223 complete AGEs were recorded. Previous studies found that the near-field AGE waveform mainly consists of two parts, the main pulse and low-frequency bubble signal 2. However, we found that the near-field AGE signal recorded by DAS has no main pulse (Fig. S1 in the supporting information), and the similarity of different AGEs was less than 20% (Fig. S2 in the supporting information). The main reason for this phenomenon may be that the observation distance was too short, and the DAS record was clipped.

We also conducted ten hammering experiments to measure the velocity of seismic waves propagating in the ice. The main energy of hammering signal is above 100 Hz (Fig. S1 in the supporting information). A relatively weak P wave signal can be seen in the DAS record on the ice surface. Using the DAS record in a line with the hammering point, we estimated that the P wave velocity in the ice is ~3200 m/s (Fig. S3 in the supporting information), which is consistent with previous studies (e.g., Castongia et al., 2017).

Besides the AGE and hammering signals, we observed two types of passive source signals (Fig. 2). The first kind is icequake within the ice plate dominated by energy at high frequency (from >10 Hz to a few hundreds of Hz (Fig. 2). They correspond to longitudinal waves in the and the elongation associated with flexural waves which propagate along the fiber direction (Moreau et al., 2020). When some icequakes occurred, the staff also heard the cracking sound, consistent with previous observations (Kavanaugh et al., 2018). The other kind, termed as Low Frequency Event (LFE) (Fig. 2), is dominated by energy in the lower frequency band (1-10 Hz) and has a duration of nearly 1 s. These LFEs, emerging primarily after AGEs, share very similar waveforms and moveouts (Fig. S4 in the supporting information).

4 Seismic events detection

Using an AI based method You Only See Once (YOLO) (Redmon and Farhadi, 2018), we scan efficiently through the DAS data (see Appendix A). The AGE catalogue indicates the accuracy of the detection method. To further determine the mechanism of the seismic sources, we locate the detected icequakes and LFEs, respectively (see Appendix B). We detected 14,498 icequakes, exhibiting a clear diurnal cycle (Fig. 2c) and primarily clustered along the promising fractures (Fig. 2d). The number of icequakes does not seem to be associated with AGEs but is rather correlated with the local temperature

https://doi.org/10.5194/tc-2023-26
Preprint. Discussion started: 21 February 2023

variation (Fig. 2c), consistent with other studies (e.g., Kavanaugh et al., 2018). The icequake interevent distribution follows a Poisson distribution (Fig. S5 in the supporting information), indicating its randomness, similar to tectonic earthquakes (Rydelek and Sacks, 1989). These observations reveal the nature of icequakes in our experiments as brittle failure of ice plate caused by uneven thermal expansion. Thus, the surge of icequake activity since the noon of January 9th probably indicates a heightened development of cracks within the ice plate. There also seems to be a slight delay between the icequake activity and the temperature, which is probably due to lag from thermal diffusion. However, a robust establishment on the relationship requires a longer observation.

A total of 9,391 LFEs are detected, mostly clustered in the centre of the lake, and close to the airgun floating platform (Fig. 2d). LFEs tend to follow the AGEs tightly (although vary in detectable numbers for different AGEs depending on noise levels), and are difficult to observe 5 minutes after AGEs (Fig 2c and Fig. S6 in the supporting information). The occurrence of LFEs does not follow a Poisson distribution (Fig. S7 in the supporting information), indicating that they are not random events but likely triggered by the water vibration following the AGEs that has been widely observed.

5 Dispersion curve of LFE

To gain a deeper understanding of the physical mechanism of LFEs and its signal propagation, we extract the dispersion relation from the waveforms of LFEs. Since the LFEs share rather similar waveforms and moveout pattern (Fig. S4 in the supporting information), we take a master LFE event and stack the waveforms of other LFEs with time shift measured via cross correlating to enhance the signal-to-noise ratio (SNR). As a quality control, we only retain waveforms with cross-correlation coefficient greater than 0.7 and the resulting stacked waveforms are shown in Fig. 3 with a clear inverse dispersion. We then apply the multi-channel surface wave analysis method (Park et al., 1999) on the stacked LFE waveforms and extract the phase velocity dispersion curve. The phase velocity increases with frequency and varies from 20 to 160 m/s in 1 to 15 Hz (Fig. 3c), much lower than the typical shear wave velocity of the ice (~1400 m/s, Hudson et al., 2021). This dispersion curve has the canonical trait of a special guided wave along a suspending ice shelf driven by the interplay of ice plate flexure and gravity, namely the Flexural-Gravity Wave (FGW) (Williams and Robinson, 1981) which corresponds to the quasi-Scholte mode (QS) seismic wavefield of a floating ice plate (Moreau et al., 2020; Nziengui-Bâ et al., 2022). The dispersion of the FGW is largely controlled by the ice plate thickness and stiffness (Zhao et al., 2018; Sergienko, 2017; Sutherland & Rabault, 2016; Timco & Frederking, 1983; Yang & Yates, 1995). Given a roughly known ice plate thickness (~0.5 m), we successfully explain the observed dispersion curve using the theoretical prediction of FGW (equation 1 in reference Sutherland & Rabault, 2016, and Appendix C) with an ice Young's modulus (E) around 10 GPa.

The effective modulus can be regarded as an indicator of the elastic and viscous deformation that is dependent on the strain rate, temperature, density, ice type, purity etc. (Sinha, 1989). And the Young's Modulus for different types of ice is very similar at a constant temperature. In the study of Nziengui-Bâ et al. (2022), the Young's Modulus are below 5 GPa. They suspected that the value of E is underestimated due to snow layer covering the ice surface or inhomogeneity/porosity of

https://doi.org/10.5194/tc-2023-26
Preprint. Discussion started: 21 February 2023

the solid columnar ice layer. In this study, the lake surface is covered with clear ice, implying a stronger stiffness, which is consistent with previous researches (Gold, 1988; Northwood, 1947; Petrovic, 2003).

6 Discussion

In this study the seismic events are detected and located with dense DAS array, which has a promising high detection ability. As a comparison, we detect seismic events using one reference seismometer onshore with another deep-neural-network-based seismic arrival picking method (PhaseNet) (Zhu and Beroza, 2019). A total of 2,348 events are detected (Fig. S8 in the supporting information), and all of them agreed well with icequakes detected on DAS record by YOLO but about 6 times fewer. Applying PhaseNet on a single channel of DAS (channel 150) does result in more detected events than the record from the onshore seismometer (Fig. S8 in the supporting information) but also with a higher false detection rate, probably because PhaseNet was not trained with icequake data. Moreover, through visual inspection, we also confirmed that none of the LFEs were detected by PhaseNet. This is not unexpected as PhaseNet was trained with tectonic earthquake data, which share more similarity with icequakes than LFEs. In the future, DAS records may be added to the training set of PhaseNet and improve the performance in detecting icequakes and LFEs. The delay of the icequakes occurrence and the temperature may be probably due to lag from thermal diffusion. We did not directly measure the ice temperature but used the temperature data of the air. Future work warrants a combined distributed temperate sensing (DTS) (Selker et al., 2006) and DAS in-situ observation to provide a more accurate connection between temperature and seismic activity. Besides, a more complex distribution of the optic fibre, for example, the Zig-Zag array used in the PoroTomo project (Parker et al., 2018), can improve seismic event detection and location.

Deformation induced by ocean waves (e.g., FGW) have a significant impact on ice shelf stability and may even lead to its fragmentation or trigger calving (Collins III et al., 2015; Liu and Mollo-Christensen, 1988), however, direct observations of the FGW dispersion remained limited in previous studies (Sutherland and Rabault, 2016). Fichtner et al. (2022) recorded FGW with DAS on the ice cap of a volcano, they explained it as low-frequency volcanic tremor. In this work, we obtain the DAS record of clear FGW and estimate the ice stiffness as the plate thickness is known. In practice, the thickness and stiffness can be estimated simultaneously under a Bayesian scheme (Nziengui-Bâ et al., 2022), which is very valuable on ice shelf where the thickness is not well resolved. Therefore, accurate record of FGW on DAS would be useful for inferring both the ice shelf thickness and ice stiffness. For a cracked ice plate, the stiffness usually decreases, compare to the elastic modulus of the grains (12 GPa), implying the thickness of the grain boundaries can be probably estimated with the effective value of the modulus (Wang et al., 2008). Due to the AGE, the ice plate close to the AirGun floating platform was severely fractured (Fig. 1) which implies that the Young's Modulus may be smaller than that of the other places. We measured the dispersion curves of FGW for inner circle and outer circle of the optical cable DAS records. The results support our speculation (Fig. S9 in the supporting information), which also explain the low phase velocity of FGW around 10 Hz in Fig. 3c. The dispersion curve of FGW measured with hammer signal (red triangle in Fig. 1) also indicates a smaller E (Fig. S10

https://doi.org/10.5194/tc-2023-26
Preprint. Discussion started: 21 February 2023

in the supporting information). The E is close to 7.5 GPa in the inner circle, which is probably due to intense fractures. Our experiment is limited to a 3-day period on a frozen lake of a few hundred of meters. However, it is possible to monitor the temporal change in stiffness or thickness of the ice shelf plate with longer continuous observation time of the LFE. One may also expect to capture the attenuation (Yang and Yates, 1995) effect upon deploying a longer DAS cable.

Previous studies have shown that FGW can trigger icequakes on the ice shelf. For example, Zhao et al. (2019) found seismicity of icequakes exhibits spatial and seasonal associations with ocean gravity wave, thus affecting the integrity of the ice shelf and increasing the risk of ice shelf disintegration (Zhao et al., 2019). Olinger et al. found thermal and tidal stresses are important in generating icequakes on the shelf (Olinger et al., 2019). During our experiment, the number of icequakes after the AGE did not change significantly (Fig. S11 in the supporting information), indicating the airgun shot or the FGW are probably not strongly correlated with icequakes. The number of icequakes even decreases slightly after the AGE, which may due to detection capability reduced by strong AGE coda. This discrepancy may reflect structural difference between the ice plate on a frozen lake and a real ice shelf, which needs to be addressed by more on-site future seismic observations on real ice shelf.

Our work shows that DAS has important application potential to monitor the formation and development of ice cracks using passive source signals recorded in similar ice shelf studies, especially when there is firn layer on the ice and it is difficult to use optical methods. In addition, the variations of FGW can provide information of the stiffness inhomogeneity, which can probably infer the size of the ice plate fragments. Our experiment is carried out on the surface of an ice-covered lake, to make it available on ice shelf, we need first to consider the spatial sampling to optimize the array layout. For example, hundreds of meters of optical fibre can be used to locate ice quakes with meter-level accuracy, and can also measure FGW with a wavelength of dozens of meters. For an ice shelf with a thickness of hundreds of meters and a length of tens of kilometres, to measure the FGW caused by ocean waves (the corresponding wavelength is several kilometres at period longer than 10 s, Zhao et al., 2018), the spatial span of optical fibre should be several kilometres. There are other limitations that need to be addressed in the future. The conventional DAS fibre only measures a single strain component along the cable and does not provide polarization information, which increases the difficulty of identifying seismic phases (Hudson et al., 2021), and lack of horizontal shear mode enlarges the uncertainty of ice properties estimation (Nziengui-Bâ et al., 2022). One remedy is use helically wound fibre but challenging for data processing (Ning and Sava, 2018). Moreover, DAS array on the seafloor is necessary to monitor the ocean wave and study the response of the ice shelf to the ocean waves (Lindsey et al., 2019).

7 Conclusion

In this work, we deployed a dense DAS network on a frozen lake and captured abundant near-field seismic signals produced by cracking (icequakes) and dynamic flexure (LFEs) of the ice plate. The icequakes, accompanied by audible cracking sounds, clearly delineates the fractures on the ice plate. The LFEs correspond to propagating FGWs and provide a

https://doi.org/10.5194/tc-2023-26
Preprint. Discussion started: 21 February 2023

tight constraint on the ice stiffness. Thus, the DAS array constitutes an exceptional technology for mapping internal fractures and monitoring the strength of ice shelf. Combined with other remote sensing observations (Massom et al., 2018), DAS has a grand potential in understanding and monitoring ice shelf disintegration.

Appendix A: Seismic event detection based on YOLO

We convert the record section of DAS waveforms to images and apply a convolutional neural network (CNN) You Only See Once (YOLO, version 5) to detect the seismic events and classify them into three categories: AGE LFE and icequake. YOLO was developed for accurate real-time object detection for video files (Redmon & Farhadi, 2018), which also has been used to detect micro-seismic event for DAS record (Stork et al., 2020). To enhance the SNR, the DAS data is bandpass filtered to 5-50 Hz and normalized with respect to the maximum amplitude of the entire record section. We assemble 6-second data of all channels (51-645) into an image with 50% overlap to prevent misdetection. We then down sample the image to 600 by 600 pixels and keep each image size to about 980 KB.

To train the AI model, we manually inspected the seismic data of the first 12 hours and labelled 60 AGEs,122 LFEs and 360 icequakes. We then divide this dataset into training, validation, and test sets in a 4:1:1 ratio. The catalog of AGE is known and mainly used to evaluate the performance of the model. We used GPU to accelerate the training (took ~3 hours) and the model's performance on the test set is shown in Fig. S12. The confusion rate is low for example, no AGE was detected as icequake. The recall rates for AGEs, LFEs and icequakes are 100.0%, 100.0% and 91.0%, while the accuracy rates for the three are 73.0%, 93.0% and 62.8%, respectively. Finally, we apply trained AI model to scan through the rest of the seismic data (39,280 images). In total, we detected 14,498 icequakes and 9,391 LFEs.

Appendix B: Seismic event location

We locate the seismic events using an absolute location method based on the neighbourhood algorithm (Sambridge, 1999) with the first arrivals. We assumed a constant seismic velocity in all directions, since the structure of the site is relatively simple, and set it as an inversion parameter. Since the ice plate is thin, we assume the focal depth to be zero. We used a STA/LTA method (Stevenson, 1976) to pick arrivals. The short and long time-windows are set to 0.05 s and 0.25 s for icequakes, and 0.5 s and 2.5 s for LFEs, respectively. To make full use of the waveform information, the error of the travel time misfit is normalized by the maximum amplitude of each waveform. We locate 10 hammering events to assess the location error. The minimum, maximum and average location errors of hammering event are 5 m, 20 m and 10.2 m (Fig. S13 in the supporting information). However, most results were biased to the north. This systematic deviation may be caused by the systematic bias in the position of optical fiber, and by the number and accuracy of arrival picks.

https://doi.org/10.5194/tc-2023-26
Preprint. Discussion started: 21 February 2023

Appendix C: Dispersion relation of FGW

The dispersion relation (relation of frequency (f) and wavenumber (k)) for FGW can be written as,

$$(2\pi f)^2 = \frac{(gk+Dk^5-Qk^3)}{\coth kH+kM} \quad (1).$$

g is gravity, k is wavenumber, H is the water depth which is 60 meters in this study. D is the bending modulus, which is a function of ice properties, $D = Eh^3/\rho_w 12(1-v^2)$, where E is the Young's modulus, υ is the Poisson ratio, h is the ice thickness which is 0.5 meters in this study, ρ_w is the density of water. Q is due to compression forces, $Q = Ph/\rho_i$, where ρ_i is the density of ice. M is due to the added mass of the ice sheet, $M = h\rho_i/\rho_w$. Q and M are much smaller than gravity and flexural terms and can be neglected. The dispersion equation can be rewritten as,

$$(2\pi f)^2 = \frac{(gk+k^5 Eh^3/\rho_w 12(1-v^2))}{\coth kH} \quad (2).$$

The Young's Modulus can also be determined with compressional wave velocity Vp, $E = V_P^2(1-v^2)$, assuming v=0.33, according to the results from Fig. S3, E is 9.12 GPa.

Data availability

All raw data can be provided by the corresponding authors upon request.

Author contributions

XZ, SN planned the campaign; RL performed the measurements; JX, XZ, CL, FB and HL analysed the data; JX wrote the manuscript draft; JX, XZ, CL, SN, RC, BC and FB reviewed and edited the manuscript.

Competing interests

The authors declare that they have no conflict of interest.

Acknowledgements

The authors thank Baoshan Wang, Rui Zou, Yahong Wang for their help on the experiment setup and data requisition. We thank Herb Wang and Daoyuan Sun for their professional suggestions.

https://doi.org/10.5194/tc-2023-26
Preprint. Discussion started: 21 February 2023

Financial support

This work was supported by the National Natural Science Foundation of China with grant number 42274076.

References

Aster, R. C. and Winberry, J. P.: Glacial seismology, Rep. Prog. Phys., 80, 126801, https://doi.org/10.1088/1361-6633/aa8473, 2017.

Booth, A. D., Christoffersen, P., Schoonman, C., Clarke, A., Hubbard, B., Law, R., Doyle, S. H., Chudley, T. R., and Chalari, A.: Distributed Acoustic Sensing of Seismic Properties in a Borehole Drilled on a Fast-Flowing Greenlandic Outlet Glacier, Geophys. Res. Lett., 47, e2020GL088148, https://doi.org/10.1029/2020GL088148, 2020.

Brisbourne, A. M., Kendall, M., Kufner, S.-K., Hudson, T. S., and Smith, A. M.: Downhole distributed acoustic seismic profiling at Skytrain Ice Rise, West Antarctica, Cryosphere, 15, 3443–3458, https://doi.org/10.5194/tc-15-3443-2021, 2021.

Castongia, E., Wang, H. F., Lord, N., Fratta, D., Mondanos, M., and Chalari, A.: An Experimental Investigation of Distributed Acoustic Sensing (DAS) on Lake Ice, JEEG, 22, 167–176, https://doi.org/10.2113/JEEG22.2.167, 2017.

Chen, Z., Bromirski, P. D., Gerstoft, P., Stephen, R. A., Wiens, D. A., Aster, R. C., and Nyblade, A. A.: Ocean-excited plate waves in the Ross and Pine Island Glacier ice shelves, J. Glaciol., 64, 730–744, https://doi.org/10.1017/jog.2018.66, 2018.

Chen, Z., Bromirski, P. D., Gerstoft, P., Stephen, R. A., Lee, W. S., Yun, S., Olinger, S. D., Aster, R. C., Wiens, D. A., and Nyblade, A. A.: Ross Ice Shelf Icequakes Associated With Ocean Gravity Wave Activity, Geophys. Res. Lett., 46, 8893–8902, https://doi.org/10.1029/2019GL084123, 2019.

Collins III, C. O., Rogers, W. E., Marchenko, A., and Babanin, A. V.: In situ measurements of an energetic wave event in the Arctic marginal ice zone, Geophys. Res. Lett., 42, 1863–1870, https://doi.org/10.1002/2015GL063063, 2015.

Dobretsov, N. L., Ruzhich, V. V., Psakhie, S. G., Chernykh, E. N., Shilko, E. V., Levina, E. A., and Ponomareva, E. I.: Advance in earthquake prediction by physical simulation on the baikal ice cover, Phys Mesomech, 16, 52–61, https://doi.org/10.1134/S1029959913010062, 2013.

Ekström, G., Nettles, M., and Abers, G. A.: Glacial Earthquakes, Science, 302, 622–624, https://doi.org/10.1126/science.1088057, 2003.

Fichtner, A., Klaasen, S., Thrastarson, S., Çubuk-Sabuncu, Y., Paitz, P., and Jónsdóttir, K.: Fiber-Optic Observation of Volcanic Tremor through Floating Ice Sheet Resonance, The Seismic Record, 2, 148–155, https://doi.org/10.1785/0320220010, 2022.

Gold, L. W.: On the elasticity of ice plates, Can. J. Civ. Eng., 15, 1080–1084, https://doi.org/10.1139/l88-140, 1988.

de Graaf, K. L., Brandner, P. A., and Penesis, I.: The pressure field generated by a seismic airgun, Exp. Therm. Fluid Sci., 55, 239–249, https://doi.org/10.1016/j.expthermflusci.2014.02.025, 2014.

Helmstetter, A., Nicolas, B., Comon, P., and Gay, M.: Basal icequakes recorded beneath an Alpine glacier (Glacier d'Argentière, Mont Blanc, France): Evidence for stick-slip motion?, J. Geophys. Res-Earth, 120, 379–401, https://doi.org/10.1002/2014JF003288, 2015.

https://doi.org/10.5194/tc-2023-26
Preprint. Discussion started: 21 February 2023

Hudson, T. S., Baird, A. F., Kendall, J. M., Kufner, S. K., Brisbourne, A. M., Smith, A. M., Butcher, A., Chalari, A., and Clarke, A.: Distributed Acoustic Sensing (DAS) for Natural Microseismicity Studies: A Case Study From Antarctica, J. Geophys. Res-Sol Ea., 126, e2020JB021493, https://doi.org/10.1029/2020JB021493, 2021.

Kavanaugh, J., Schultz, R., Andriashek, L. D., van der Baan, M., Ghofrani, H., Atkinson, G., and Utting, D. J.: A New Year's Day icebreaker: icequakes on lakes in Alberta, Canada, Can. J. Earth Sci., 56, 183–200, https://doi.org/10.1139/cjes-2018-0196, 2018.

Köhler, A., Maupin, V., Nuth, C., and Pelt, W. van: Characterization of seasonal glacial seismicity from a single-station on-ice record at Holtedahlfonna, Svalbard, Ann. Glaciol., 60, 23–36, https://doi.org/10.1017/aog.2019.15, 2019.

Lindsey, N. J., Dawe, T. C., and Ajo-Franklin, J. B.: Illuminating seafloor faults and ocean dynamics with dark fiber distributed acoustic sensing, Science, 366, 1103–1107, https://doi.org/10.1126/science.aay5881, 2019.

Liu, A. K. and Mollo-Christensen, E.: Wave Propagation in a Solid Ice Pack, J. Phys. Oceanogr., 18, 1702–1712, https://doi.org/10.1175/1520-0485(1988)018<1702:WPIASI>2.0.CO;2, 1988.

Lombardi, D., Gorodetskaya, I., Barruol, G., and Camelbeeck, T.: Thermally induced icequakes detected on blue ice areas of the East Antarctic ice sheet, Ann. Glaciol., 60, 45–56, https://doi.org/10.1017/aog.2019.26, 2019.

Massom, R. A., Scambos, T. A., Bennetts, L. G., Reid, P., Squire, V. A., and Stammerjohn, S. E.: Antarctic ice shelf disintegration triggered by sea ice loss and ocean swell, Nature, 558, 383–389, https://doi.org/10.1038/s41586-018-0212-1, 2018.

Moreau, L., Boué, P., Serripierri, A., Weiss, J., Hollis, D., Pondaven, I., Vial, B., Garambois, S., Larose, É., Helmstetter, A., Stehly, L., Hillers, G., and Gilbert, O.: Sea Ice Thickness and Elastic Properties From the Analysis of Multimodal Guided Wave Propagation Measured With a Passive Seismic Array, J. Geophys. Res-Oceans, 125, e2019JC015709, https://doi.org/10.1029/2019JC015709, 2020.

Ning, I. L. C. and Sava, P.: High-resolution multi-component distributed acoustic sensing, Geophys. Prospect, 66, 1111–1122, https://doi.org/10.1111/1365-2478.12634, 2018.

Northwood, T. D.: Sonic determination of the elastic properties of ice, Can. J. Res., 25a, 88–95, https://doi.org/10.1139/cjr47a-011, 1947.

Nziengui-Bâ, D., Coutant, O., Moreau, L., and Boué, P.: Measuring the thickness and Young's modulus of the ice pack with DAS, a test case on a frozen mountain lake, Geophys. J. Int., ggac504, https://doi.org/10.1093/gji/ggac504, 2022.

Olinger, S. D., Lipovsky, B. P., Wiens, D. A., Aster, R. C., Bromirski, P. D., Chen, Z., Gerstoft, P., Nyblade, A. A., and Stephen, R. A.: Tidal and Thermal Stresses Drive Seismicity Along a Major Ross Ice Shelf Rift, Geophys. Res. Lett., 46, 6644–6652, https://doi.org/10.1029/2019GL082842, 2019.

Park, C. B., Miller, R. D., and Xia, J.: Multichannel analysis of surface waves (MASW), Geophysics, 64, 800–808, 1999.

Parker, L. M., Thurber, C. H., Zeng, X., Li, P., Lord, N. E., Fratta, D., Wang, H. F., Robertson, M. C., Thomas, A. M., Karplus, M. S., Nayak, A., and Feigl, K. L.: Active-Source Seismic Tomography at the Brady Geothermal Field, Nevada, with Dense Nodal and Fiber-Optic Seismic Arrays, Seismol. Res. Lett., 89, 1629–1640, https://doi.org/10.1785/0220180085, 2018.

Petrovic, J. J.: Review Mechanical properties of ice and snow, J. Mater. Sci., 38, 1–6, https://doi.org/10.1023/A:1021134128038, 2003.

Podolskiy, E. A. and Walter, F.: Cryoseismology, Rev. Geophys., 54, 708–758, https://doi.org/10.1002/2016RG000526, 2016.

Redmon, J. and Farhadi, A.: YOLOv3: An incremental improvement, ArXiv, abs/184.02767, 2018.

Romeyn, R., Hanssen, A., Ruud, B. O., Stemland, H. M., and Johansen, T. A.: Passive seismic recording of cryoseisms in Adventdalen, Svalbard, Cryosphere, 15, 283–302, https://doi.org/10.5194/tc-15-283-2021, 2021.

Röösli, C., Walter, F., Husen, S., Andrews, L. C., Lüthi, M. P., Catania, G. A., and Kissling, E.: Sustained seismic tremors and icequakes detected in the ablation zone of the Greenland ice sheet, J. Glaciol., 60, 563–575, https://doi.org/10.3189/2014JoG13J210, 2014.

Ruzhich, V. V., Psakhie, S. G., Chernykh, E. N., Bornyakov, S. A., and Granin, N. G.: Deformation and seismic effects in the ice cover of Lake Baikal, Russ. Geol. Geophys., 50, 214–221, https://doi.org/10.1016/j.rgg.2008.08.005, 2009.

Rydelek, P. A. and Sacks, I. S.: Testing the completeness of earthquake catalogues and the hypothesis of self-similarity, Nature, 337, 251–253, https://doi.org/10.1038/337251a0, 1989.

Selker, J., van de Giesen, N., Westhoff, M., Luxemburg, W., and Parlange, M. B.: Fiber optics opens window on stream dynamics, Geophys. Res. Lett., 33, https://doi.org/10.1029/2006GL027979, 2006.

Sergeant, A., Mangeney, A., Yastrebov, V. A., Walter, F., Montagner, J.-P., Castelnau, O., Stutzmann, E., Bonnet, P., Ralaiarisoa, V. J.-L., Bevan, S., and Luckman, A.: Monitoring Greenland ice sheet buoyancy-driven calving discharge using glacial earthquakes, Ann. Glaciol., 60, 75–95, https://doi.org/10.1017/aog.2019.7, 2019.

Sergienko, O. V.: Behavior of flexural gravity waves on ice shelves: Application to the Ross Ice Shelf, J. Geophys. Res-Oceans, 122, 6147–6164, https://doi.org/10.1002/2017JC012947, 2017.

Sinha, N. K.: Elasticity of natural types of polycrystalline ice, Cold Reg. Sci. Technol., 17, 127–135, https://doi.org/10.1016/S0165-232X(89)80003-5, 1989.

Sutherland, G. and Rabault, J.: Observations of wave dispersion and attenuation in landfast ice, J. Geophys. Res-Oceans, 121, 1984–1997, https://doi.org/10.1002/2015JC011446, 2016.

Timco, G. W. and Frederking, R. M. W.: Flexural strength and fracture toughness of sea ice, Cold Reg. Sci. Technol., 8, 35–41, https://doi.org/10.1016/0165-232X(83)90015-0, 1983.

Veitch, S. A. and Nettles, M.: Assessment of glacial-earthquake source parameters, J. Glaciol., 63, 867–876, https://doi.org/10.1017/jog.2017.52, 2017.

Walter, F., Dalban Canassy, P., Husen, S., and Clinton, J. F.: Deep icequakes: What happens at the base of Alpine glaciers?, J. Geophys. Res-Earth, 118, 1720–1728, https://doi.org/10.1002/jgrf.20124, 2013.

Walter, F., Gräff, D., Lindner, F., Paitz, P., Köpfli, M., Chmiel, M., and Fichtner, A.: Distributed acoustic sensing of microseismic sources and wave propagation in glaciated terrain, Nat. Commun., 11, 2436, https://doi.org/10.1038/s41467-020-15824-6, 2020.

https://doi.org/10.5194/tc-2023-26
Preprint. Discussion started: 21 February 2023

340 Wei, C., Qin, M., Zhang, Y., Zou, R., Wang, L., Guo, X., Liu, X., Wang, Y., and Sun, D.: Airgun Excitation Experiments at Different Placement Depths in the Qilian Mountain of Gansu Province, China, Seismol. Res. Lett., 89, 974–982, https://doi.org/10.1785/0220170253, 2018.

West, M. E., Larsen, C. F., Truffer, M., O'Neel, S., and LeBlanc, L.: Glacier microseismicity, Geology, 38, 319–322, https://doi.org/10.1130/G30606.1, 2010.

345 Williams, R. T. and Robinson, E. S.: Flexural waves in the Ross Ice Shelf, J. Geophys. Res-Oceans, 86, 6643–6648, https://doi.org/10.1029/JC086iC07p06643, 1981.

Yang, T. C. and Yates, T. W.: Flexural waves in a floating ice sheet: Modeling and comparison with data, J. Acoust. Soc. Am., 97, 971–977, https://doi.org/10.1121/1.412076, 1995.

Zhu, W. and Beroza, G. C.: PhaseNet: a deep-neural-network-based seismic arrival-time picking method, Geophys. J. Int., 350 216, 261–273, https://doi.org/10.1093/gji/ggy423, 2019.

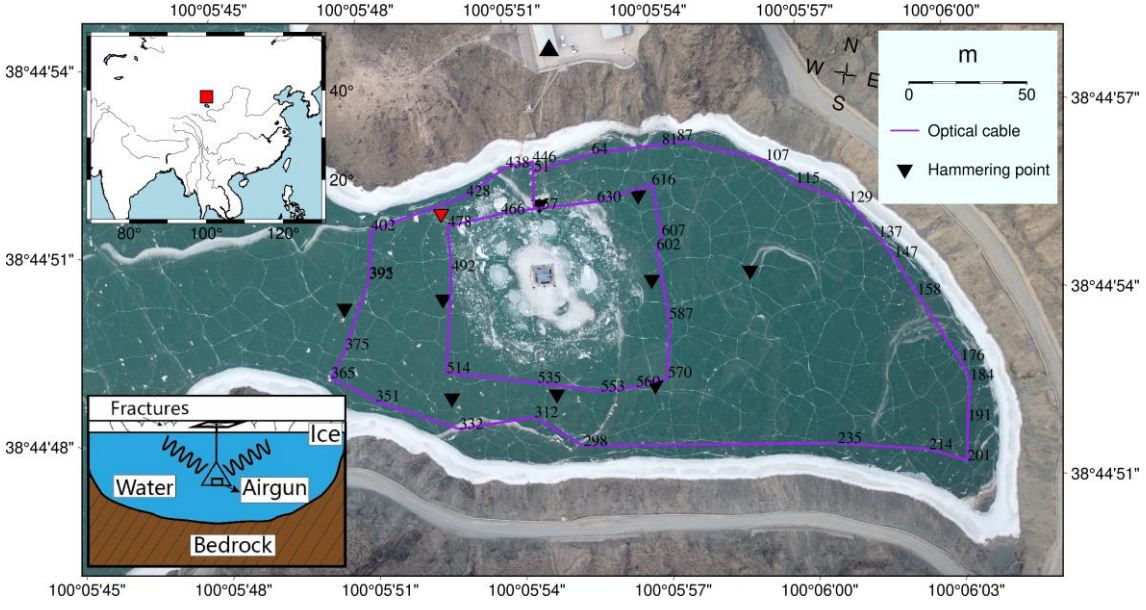

Figure 1: The experimental setting. The instrumented frozen lake is at Xiliushui Reservoir in Gansu Province, China (red 355 **rectangle in the inset). The optical fibre is marked with purple lines with channel number between 51-645 with gauge length of 10 m and a sampling rate of 1000 Hz. The airgun floating platform is at the centre of the lake. A reference broadband seismic station is marked with a triangle. Hammering points are marked with inverted triangles. The red triangle shows the one we use to measure the dispersion curve of flexural-gravity wave.**

https://doi.org/10.5194/tc-2023-26
Preprint. Discussion started: 21 February 2023

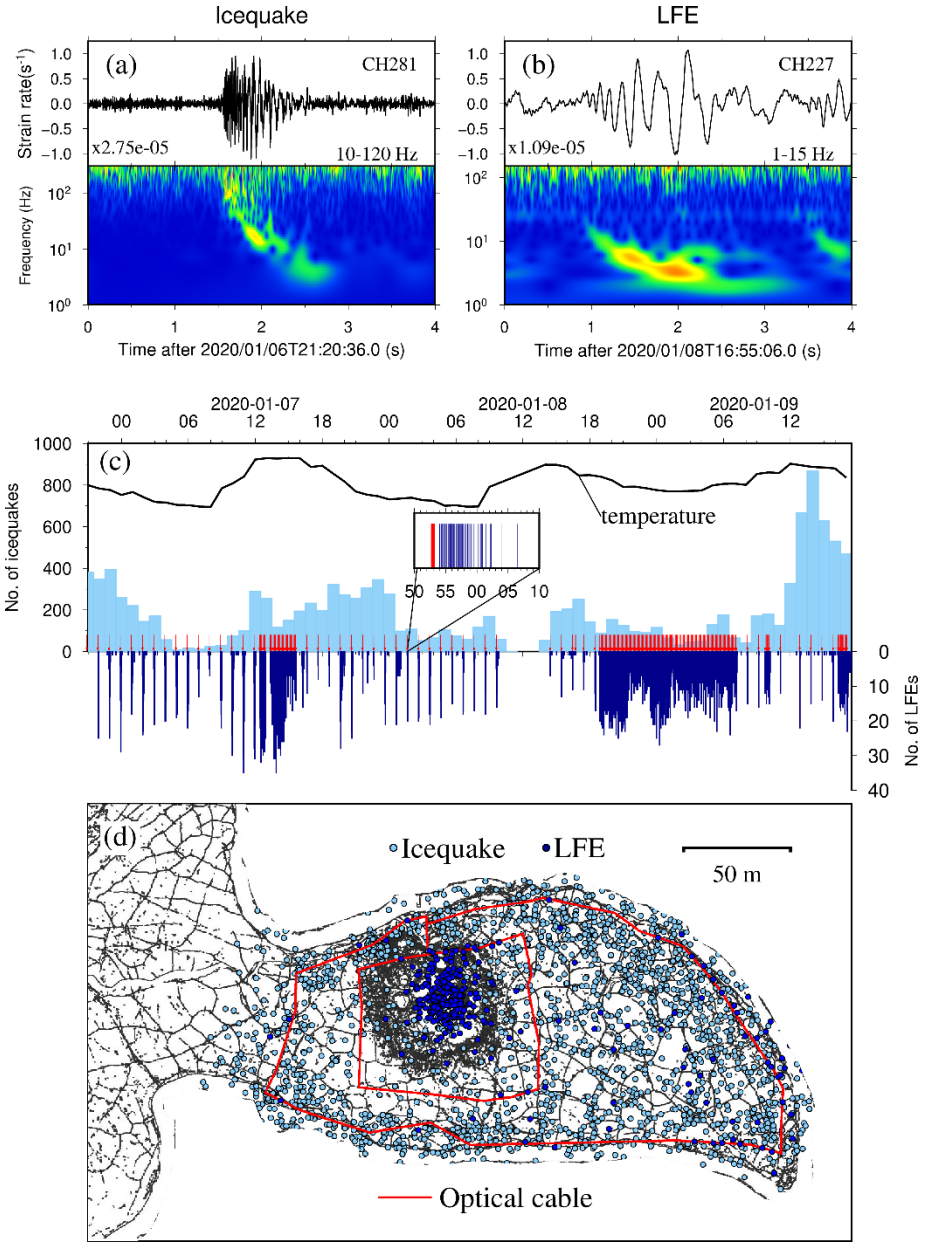

Figure 2: Typical passive signal waveforms, temporal and spatial distributions. (a) Icequake wave recorded by channel 281. The waveform is bandpass filtered in the frequency band of 10-120 Hz. (b) LFE waveform by channel 227. The waveform is bandpass filtered in the frequency band of 1-15 Hz. (c) temporal distributions for icequakes (light blue) per hour and LFEs (dark blue) per minute. The time of AGE is marked with red arrow. The inset picture shows a window of 20 minutes with an AGE (red line) and following LFEs (black lines). The air temperature is denoted with black curve. (d) spatial distribution for icequakes (light blue) and LFEs (dark blue).

https://doi.org/10.5194/tc-2023-26
Preprint. Discussion started: 21 February 2023

The Cryosphere
Discussions
Open Access
EGU

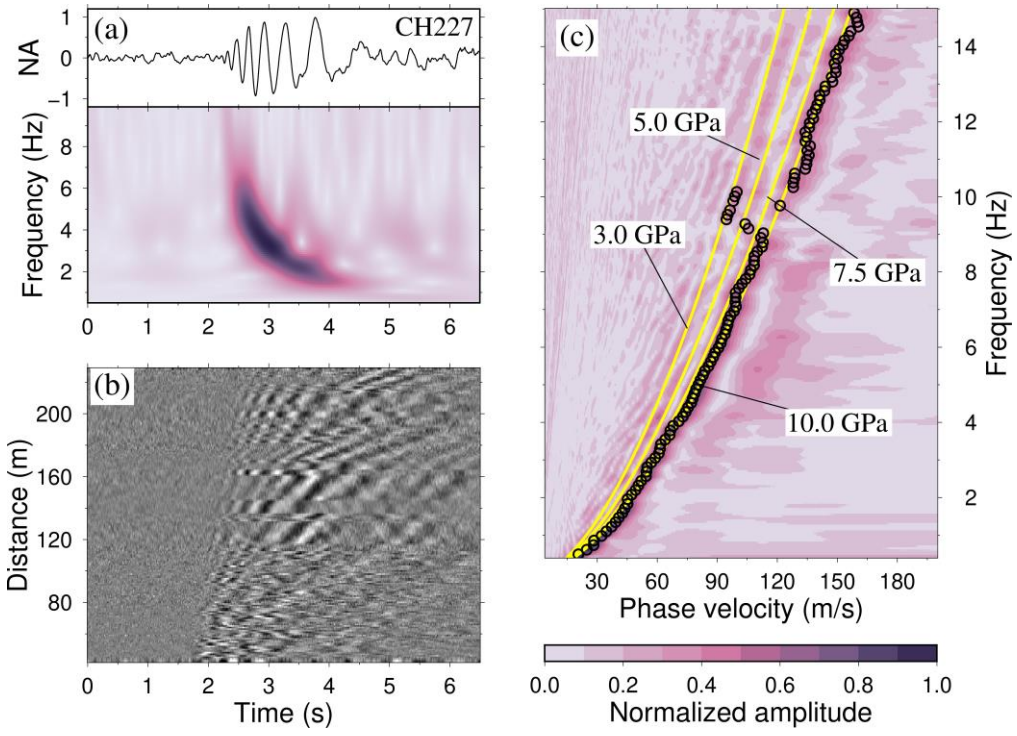

Figure 3: Dispersion analysis of LFEs. (a) Stacked LFE waveform and spectrogram of channel 227. The black curve is the stacked waveform with 272 LFE traces. It is bandpass filtered in the frequency band 1-15 Hz. The color denotes the normalized amplitude. (b) The record section of stacked waveform of all LFE events assuming all LFEs are originated at the AGE platform. (c) The measured phase velocity (circles) and predicted velocities (yellow curves) with different Young's modulus (3-10 GPa). The color means the dispersion spectra of stacked LFE traces in (c).